

Axial quasi-normal modes of neutron stars in R^2 gravity

Jose Luis Blázquez-Salcedo ^{*1}, Daniela D. Doneva ^{†2,3}, Jutta Kunz ^{‡1}, Kalin V. Staykov ^{§4}, and Stoytcho S. Yazadjiev ^{¶2,4,5}

¹Institut für Physik, Universität Oldenburg, Postfach 2503, D-26111 Oldenburg, Germany

²Theoretical Astrophysics, Eberhard Karls University of Tübingen, Tübingen 72076, Germany

³INRNE - Bulgarian Academy of Sciences, 1784 Sofia, Bulgaria

⁴Department of Theoretical Physics, Faculty of Physics, Sofia University, Sofia 1164, Bulgaria

⁵Institute of Mathematics and Informatics, Bulgarian Academy of Sciences, Acad. G. Bonchev Street 8, Sofia 1113, Bulgaria

Abstract

In the present paper the axial quasi-normal modes of neutron stars in $f(R)$ gravity are examined using a large set of equations of state. The numerical calculations are made using two different approaches – performing time evolution of the perturbation equations and solving the time-independent representation of the equations as a boundary value problem. According to the results the mode frequencies and the damping times decrease with the increase of the free parameter of the theory in comparison to the pure general relativistic case. While the frequencies deviate significantly from Einstein’s theory for all realistic neutron star masses (say above $1M_{\odot}$), the damping times reach non-negligible differences only for the more massive models. We have constructed as well universal (equation of state independent) gravitational wave asteroseismology relations involving the frequencies and the damping times. It turns out that the equation of state independence is preserved using the same normalization as in pure general relativity and the qualitative differences of the phenomenological relations with respect to Einstein’s theory of gravity can be large for large values of the free parameter in $f(R)$ gravity.

*jose.blazquez.salcedo@uni-oldenburg.de

†daniela.doneva@uni-tuebingen.de

‡jutta.kunz@uni-oldenburg.de

§kstaykov@phys.uni-sofia.bg

¶yazad@phys.uni-sofia.bg

1 Introduction

Until recently the electromagnetic channel was the only way to probe the strong field regime of gravity. This changed with the direct detection of gravitational waves from merging binary black holes [1, 2, 3, 4, 5] and binary neutron stars [6]. A very interesting fact is that in the latter case the electromagnetic counterpart was observed as well [7], which sets the beginning of the so-called multi-messenger gravitational wave astronomy. It is therefore most important to study the different sources and mechanisms for the emission of gravitational waves. A rather promising avenue here is represented by the study of quasi-normal modes (QNMs) of neutron stars. Even though such QNMs have not been detected yet, it is expected that the advance of the instruments will allow to observe them in the future. A drawback of the attempts to test the strong field regime of gravity with neutron star QNMs are the uncertainties in the nuclear matter equation of state (EOS). However, the observational constraints on the EOS are rapidly improving with time [8, 9, 10, 11, 12]. Moreover, the QNM spectrum of neutron stars is much richer than the black hole one, which offers us different possibilities to test deviations from pure general relativity (GR) (see e.g., [13, 14, 15]).

Neutron star oscillations have been studied for decades, and comprehensive classifications have been made [16, 17, 18]. In the present paper we will concentrate on the axial modes of neutron stars. (Since we will be considering nonrotating models the perturbations can be separated into purely axial and polar perturbations.) The axial modes are rapidly damped spacetime (or curvature) modes that have no analog in Newtonian gravity and are a pure manifestation of the tensorial character of GR and its generalizations similar to the QNMs of black holes [19, 20, 21]. Most of the previous studies of axial QNMs or neutron stars have been made in pure GR though. Exceptions are the studies in massless scalar-tensor theories [22], tensor-vector-scalar theory [23], Einstein-Gauss-Bonnet-dilaton gravity [24] and Horndeski gravity [25].

In the present paper we will concentrate on a class of alternative theories of gravity that attracted considerable interest recently in connection with the dark energy puzzle, and which can also produce non-negligible deviations from GR in the strong field regime, namely the $f(R)$ theories of gravity [26, 27, 28]. More precisely, we will focus on the so-called R^2 gravity having a Lagrangian of the form $f(R) = R + aR^2$, where a is a parameter, since the R^2 term is supposed to give the dominant contribution for strong fields. Realistic non-perturbative neutron star models were constructed in R^2 gravity in [29, 30, 31, 32] both in the static and rotating cases, and the results show that the deviations from GR can be significant, even though comparable with the equation of state uncertainty.

In the present paper we will perturb the non-rotating background models obtained in [29]. First we will solve the time-dependent perturbation equation to obtain the time evolution for the gravitational wave signal, extracting the oscillation frequency and the damping rate for some selected neutron star models and a realistic EOS. Then we will turn to the time-independent boundary value problem, solving for the QNMs for a large number of models and EOS. This will then allow us to address universal (EOS independent) relations for the neutron star models (see e.g. the recent reviews [33, 34]). In particular, we will investigate how GR universal relations for the rescaled frequencies and damping times [35, 36, 37, 38, 39, 40]

generalize to $f(R)$ theory.

The outline of the paper is as follows: In Section II the basic equations for the axial perturbations in $f(R)$ gravity and some notes on the numerical methods are presented. In Section III the numerical results are presented and discussed. The paper ends with a conclusion.

2 Basics

2.1 Background solution

In this paper we study the axial perturbations of neutron stars in $f(R)$ gravity with Lagrangian $f(R) = R + aR^2$, also known as R -squared gravity. For mathematical simplicity we will not work directly with the $f(R)$ gravity action and field equations, but instead we will exploit the mathematical equivalence between the $f(R)$ theories and a certain class of scalar-tensor theories (STT). In addition, when working with the STT representation of the $f(R)$ theories we will not employ the physical Jordan frame but instead the more convenient Einstein frame. Transformations to the relevant quantities in the physical Jordan frame will be made whenever needed. More details on this problem, including a detailed discussion of the transition from $f(R)$ to STT and the connection between the Jordan and Einstein frames can, e.g., be found in [29, 30, 31].

The general form of the Einstein frame action in STT can be written in the following form

$$S = \frac{1}{16\pi G} \int d^4x \sqrt{-g} [R - 2g^{\mu\nu} \partial_\mu \varphi \partial_\nu \varphi - V(\varphi)] + S_{\text{matter}}(A^2(\varphi)g_{\mu\nu}, \chi), \quad (1)$$

where R is the scalar curvature with respect to the Einstein frame metric $g_{\mu\nu}$, $V(\varphi)$ and $A(\varphi)$ are the potential and the coupling function of the scalar field φ , and S_{matter} is the action for the matter, which is symbolized by χ . One should note that an explicit coupling between the matter and the scalar field appears through the coupling function $A(\varphi)$ only in the Einstein frame due to the conformal transformation of the metric involved, while no such direct coupling exists in the physical Jordan frame. Therefore the weak equivalence principle is satisfied.

In the case of R^2 gravity the coupling function $A(\varphi)$ and the scalar field potential are given by [29, 30, 31]

$$A(\varphi) = e^{-\frac{1}{\sqrt{3}}\varphi}, \quad V(\varphi) = \frac{1}{4a} \left(1 - e^{-\frac{2\varphi}{\sqrt{3}}}\right)^2. \quad (2)$$

It is straightforward to show that the resulting scalar field is then massive with a mass $m_\varphi = 1/\sqrt{6a}$. However, the limiting case $a \rightarrow \infty$ corresponds to $m_\varphi = 0$, which is equivalent to a particular class of massless Brans-Dicke theories. Since a mass of the scalar field leads to a finite range of the scalar field of the order of its Compton wavelength, it effectively suppresses the deviations from pure GR. Thus the case $a \rightarrow \infty$ corresponds to the maximal

deviation from GR [29, 30, 31]. On the other hand, in the limit $a \rightarrow 0$ the scalar field mass tends to infinity, therefore the solutions tend to pure GR solutions.

The free parameter a of the theory is observationally constrained to $a \lesssim 10^{11} \text{ m}^2$, which translates in the dimensionless units used in the present paper to $a/R_g^2 \lesssim 10^5$ [41], where $R_g = 1.47664 \text{ km}$ is one half of the solar gravitational radius. In our calculations we will work with a up to $a \sim 10^5$ (in dimensionless units), i.e., cover the full observationally allowed range of a , where the upper limit then leads to the maximal deviations from GR within this theory.

In the following we will consider static and spherically symmetric solutions. Then the Einstein frame metric can be written in the following general form

$$ds^2 = -e^{2\nu} dt^2 + e^{2\lambda} dr^2 + r^2(d\theta^2 + \sin^2\theta d\phi^2). \quad (3)$$

The dimensionally reduced field equations in the Einstein frame, obtained after varying the action (1), are given by

$$\frac{1}{r^2} \frac{d}{dr} [r(1 - e^{-2\lambda})] = 8\pi G A^4(\varphi) \bar{\rho} + e^{-2\lambda} \left(\frac{d\varphi}{dr} \right)^2 + \frac{1}{2} V(\varphi), \quad (4)$$

$$\frac{2}{r} e^{-2\lambda} \frac{d\nu}{dr} - \frac{1}{r^2} (1 - e^{-2\lambda}) = 8\pi G A^4(\varphi) \bar{p} + e^{-2\lambda} \left(\frac{d\varphi}{dr} \right)^2 - \frac{1}{2} V(\varphi), \quad (5)$$

$$\frac{d^2\varphi}{dr^2} + \left(\frac{d\nu}{dr} - \frac{d\lambda}{dr} + \frac{2}{r} \right) \frac{d\varphi}{dr} = 4\pi G \alpha(\varphi) A^4(\varphi) (\bar{\rho} - 3\bar{p}) e^{2\lambda} + \frac{1}{4} \frac{dV(\varphi)}{d\varphi} e^{2\lambda}, \quad (6)$$

$$\frac{d\bar{p}}{dr} = -(\bar{\rho} + \bar{p}) \left(\frac{d\nu}{dr} + \alpha(\varphi) \frac{d\varphi}{dr} \right), \quad (7)$$

where $\alpha(\varphi) = \frac{d \ln A(\varphi)}{d\varphi}$. The quantities $\bar{\rho}$ and \bar{p} are the energy density and the pressure in the Jordan frame, and they are connected to the respective quantities in the Einstein frame via $\rho = A^4(\varphi) \bar{\rho}$ and $p = A^4(\varphi) \bar{p}$.

In order to obtain neutron star solutions, this system of field equations (4) has to be supplemented by an equation of state for the matter in the Jordan frame of the form $\bar{p}(\bar{\rho})$. The boundary conditions are chosen to imply regularity at the center of the star and asymptotic flatness at spatial infinity. Thus we impose at the center $\bar{\rho}(0) = \bar{\rho}_c$, $\lambda(0) = 0$ and $\frac{d\varphi}{dr}(0) = 0$, where $\bar{\rho}_c$ is a free parameter denoting the central energy density. The condition $\frac{d\varphi}{dr}(0) = 0$ ensures the regularity of the corresponding scalar field in both (Einstein and Jordan) frames. The Jordan and the Einstein metrics are conformally equivalent, and therefore the condition $\lambda(0) = 0$ at $r = 0$ secures regularity of the geometry in both frames. The boundary conditions at infinity, which lead to asymptotic flatness in both frames, are $\lim_{r \rightarrow \infty} \nu(r) = 0$, and $\lim_{r \rightarrow \infty} \varphi(r) = 0$.

Let us comment on how do we calculate the physical distance from the center of the compact object to a fixed point, since this will be used later. It would be different from the Einstein frame distance, and it is computed in the following way

$$r_{\text{phys}} = \int_0^r A(\varphi) e^\lambda dr, \quad (8)$$

which follows from the fact that the coupling function $A(\varphi)$ is actually the conformal factor connecting the metrics of the Jordan frame and the Einstein frame. Another quantity that should be evaluated in the physical Jordan frame is the physical radius of the star, which is determined by the requirement that the pressure should vanish at the stellar surface $r_S = r(\bar{p} = 0)$. It is easily seen that the physical radius is given by $R_S = A(\varphi_S)r_S$, where φ_S is the value of the scalar field at the stellar surface. The neutron star mass on the other hand is the same in both frames [29]. Likewise, the frequencies and damping times of the QNMs are the same in the Jordan frame and in the Einstein frame.

2.2 Axial perturbations and exterior complex scaling

Following the standard procedure [16, 17, 18] the axial perturbations of the metric can be written as

$$H_{\mu\nu}^{axial} = \begin{pmatrix} 0 & 0 & h_0(t, r)S_\theta^{lm}(\theta, \phi) & h_0(t, r)S_\phi^{lm}(\theta, \phi) \\ 0 & 0 & h_1(t, r)S_\theta^{lm}(\theta, \phi) & h_1(t, r)S_\phi^{lm}(\theta, \phi) \\ h_0(t, r)S_\theta^{lm}(\theta, \phi) & h_1(t, r)S_\theta^{lm}(\theta, \phi) & 0 & 0 \\ h_0(t, r)S_\phi^{lm}(\theta, \phi) & h_1(t, r)S_\phi^{lm}(\theta, \phi) & 0 & 0 \end{pmatrix}, \quad (9)$$

where $(S_\theta^{lm}(\theta, \phi), S_\phi^{lm}(\theta, \phi)) = (-\partial_\phi Y_{lm}(\theta, \phi)/\sin\theta, \sin\theta\partial_\theta Y_{lm}(\theta, \phi))$ with $Y_{lm}(\theta, \phi)$ being the spherical harmonics. Since the scalar field φ , the pressure p and the energy density ρ transform as true scalars under reflections of the angular coordinates their axial perturbations vanish.

The relevant perturbed field equations are then given by

$$-e^{-2\nu}\partial_t^2 h_1 + e^{-2\nu}\left(\partial_r - \frac{2}{r}\right)\partial_t h_0 - \frac{(l-1)(l+2)}{r^2}h_1 = 0, \quad (10)$$

$$\partial_t h_0 - e^{\nu-\lambda}\partial_r(e^{\nu-\lambda}h_1) = 0. \quad (11)$$

Extracting $\partial_t h_0$ from the second equation and substituting it into the first, we find the equation for h_1 . But instead of using h_1 it is convenient to use the function

$$X = h_1 \frac{e^{\nu-\lambda}}{r}. \quad (12)$$

In terms of the function X , the axial perturbations in $f(R)$ gravity are described by the following time-dependent equation

$$\begin{aligned} \frac{\partial^2 X}{\partial t^2} &- e^{\nu-\lambda}\frac{\partial}{\partial r}\left[e^{\nu-\lambda}\frac{\partial X}{\partial r}\right] + \\ &+ e^{2\nu}\left[\frac{l(l+1)}{r^2} - \frac{3}{r^2}(1 - e^{-2\lambda}) + 4\pi A^4(\varphi)(\bar{\rho} - \bar{p}) + \frac{1}{2}V(\varphi)\right]X = 0, \end{aligned} \quad (13)$$

where we have also used that

$$-re^{-\nu-\lambda}\frac{d}{dr}\left(\frac{e^{\nu-\lambda}}{r^2}\right) = \frac{2}{r^2} - \frac{3}{r^2}(1 - e^{-2\lambda}) + 4\pi GA^4(\varphi)(\bar{\rho} - \bar{p}) + \frac{1}{2}V(\varphi). \quad (14)$$

For the perturbation function $X(r, t)$ we can assume the usual time-dependence $X(r, t) = X(r)e^{i\omega t}$, which leads to a time-independent equation

$$e^{\nu-\lambda} \frac{d}{dr} \left[e^{\nu-\lambda} \frac{dX}{dr} \right] + \left\{ \omega^2 - e^{2\nu} \left[\frac{l(l+1)}{r^2} - \frac{3}{r^2} (1 - e^{-2\lambda}) + 4\pi A^4(\varphi)(\bar{\rho} - \bar{p}) + \frac{1}{2} V(\varphi) \right] \right\} X = 0. \quad (15)$$

The QNM frequency ω is complex, $\omega = \omega_R + i\omega_I$, where the real part ω_R corresponds to the frequency of the oscillations, while the imaginary part ω_I is the inverse of the damping time τ of the modes.

The perturbation has to be regular at the center of the star, which implies $X(r \rightarrow 0) \sim r^{l+1}$. At infinity, $r \rightarrow \infty$, the general form of the solution is a linear combination of an outgoing and an ingoing wave

$$X \sim A_{in} e^{i\omega(t+R)} + A_{out} e^{i\omega(t-R)}, \quad (16)$$

where $dR = e^{\lambda-\nu} dr$ defines the tortoise coordinate. Since we are interested in neutron star QNMs, X should have the form of a purely outgoing wave at infinity without any ingoing wave contribution. However, trying to impose this condition numerically leads to severe numerical problems. For example in the case of stable modes with $\omega_I > 0$ the outgoing perturbation diverges for large distance, while the ingoing contribution goes exponentially to zero. Thus, any small numerical contamination with an ingoing wave contribution leads to errors in the determination of the resonant frequencies.

This problem of course exists only when we solve the time-independent perturbation equation (15). If we perform a direct time evolution of the time-dependent perturbation equation (13), the outgoing wave condition does not have to be imposed explicitly. Instead, we should just locate the rightmost boundary of the integration domain far enough from the center of the star, so that any ingoing contamination of the signal would have to travel too long to the point of extraction of the gravitational wave signal and, thus, would not influence the final results.

In order to control the error coming from the numerical contamination with an ingoing wave when calculating the resonant frequencies using the time-independent perturbation equation (15), we employ the method based on exterior complex scaling (see e.g., [42, 39, 40, 24]). Instead of integrating directly Eq. (15) for the perturbation X , we consider the phase function of the perturbation. Thus we transform Eq. (15) to the form of a Riccati equation [43] by defining the phase function of the perturbation via $\frac{dX}{dr} = gX$. Then we obtain

$$\begin{aligned} \frac{dg}{dr} = & -g^2 - e^{2\lambda-2\nu} \omega^2 + g e^{2\lambda} \left[4\pi r A^4(\varphi)(\bar{\rho} - \bar{p}) + \frac{r}{2} V(\varphi) - \frac{1}{r} (1 - e^{-2\lambda}) \right] \\ & + e^{2\lambda} \left[4\pi A^4(\varphi)(\bar{\rho} - \bar{p}) + \frac{1}{2} V(\varphi) + \frac{l(l+1)}{r^2} - \frac{3}{r^2} (1 - e^{-2\lambda}) \right]. \end{aligned} \quad (17)$$

Regular perturbations at the center of the neutron star will possess a phase function behaving like $g \sim \frac{l+1}{r}$ close to $r = 0$. At infinity, however, a general solution of the equation will look

like

$$g \sim i\omega \frac{A_{in}e^{i\omega r} - A_{out}e^{-i\omega r}}{A_{in}e^{i\omega r} + A_{out}e^{-i\omega r}}, \quad (18)$$

which tends to $g|_{\infty} = -i\omega$ asymptotically, for both purely outgoing waves and mixed (ingoing plus outgoing) waves.

In order to guarantee that the solutions correspond to purely outgoing waves, we make an analytical continuation of the equation into the complex plane. This can be done by defining a complex coordinate r [44]

$$r = r_j + ye^{-i\zeta}, \quad (19)$$

where the real numbers r_j and ζ are auxiliary constants, and $y \in [0, \infty)$. The asymptotic behaviour of the phase function g then becomes for $y \rightarrow \infty$

$$g \sim i\omega \frac{A_{in}e^{i\xi y} - A_{out}e^{-i\xi y}}{A_{in}e^{i\xi y} + A_{out}e^{-i\xi y}}, \quad (20)$$

with $\xi = \xi_R + i\xi_I$ and $\xi_R = \omega_R \cos \zeta + \omega_I \sin \zeta$, $\xi_I = \omega_I \cos \zeta - \omega_R \sin \zeta$. If we now choose ζ such that $\xi_I = \omega_I \cos \zeta - \omega_R \sin \zeta < 0$, the condition $g|_{\infty} = -i\omega$ enforces $A_{in} = 0$, and the solution will describe purely outgoing waves.

With this setting, the resulting numerical procedure is the following. First we generate a static background solution, where we have to fix the parameters of the theory (i.e., the constant a), the equation of state, and the central pressure of the configuration. In the next step, we calculate the coefficients of Eq. (17) using the background configuration. Then we generate an *interior* solution of this equation extending from the center of the star at $r = 0$, up to a point at $r = r_j$, where the point r_j is chosen to be outside the star ($r_j > R_s$), and we demand regularity of the phase function by imposing $\lim_{r \rightarrow 0} r \cdot g = l + 1$.

Next, a second solution of Eq. (17) is generated, but this time after performing the transformation (18) with $\omega_I \cos \zeta - \omega_R \sin \zeta < 0$. This solution extends from $r = r_j$ to infinity, and we demand the *exterior* phase to satisfy $g|_{\infty} = -i\omega$, which imposes the outgoing wave behaviour. QNMs are obtained when the interior phase solution and the exterior phase solution are continuous at the point $r = r_j$. In our case, this only happens for a discrete set of values of ω . We implement a search algorithm that minimizes the difference between both solutions at $r = r_j$ using the gradient descent. Once we obtain a QNM, we test the numerical stability by changing the auxiliary parameters r_j and ζ . Typically the QNMs can be obtained with a relative accuracy of 10^{-3} or better.

3 Numerical results

We used two independent numerical techniques for solving the problem in order to verify the results and gain deeper insight. First we performed a time evolution of Eq. (13) perturbing the star with some initial pulse. This is the most general way of constructing a solution since

we just impose some initial perturbation, and then let the system evolve. The resulting signal will contain an admixture of all the excited modes. The drawback of this method is that it normally yields only the first axial QNM because of the short damping times of the higher axial modes. In addition, only a few oscillations can be observed before the signal dies out due to the fast damping, which leads to large errors in the extracted frequencies and damping times.

Solving the time-independent perturbation equation (15) via the complex scaling method is of course more involved, but it is a much more robust procedure, that can be used to explore the parameter space with high accuracy. Therefore, we used this method to obtain the QNMs of a large variety of EOS and extract a set of universal relations. The background solutions were obtained using the ODE solver Colsys [45]. Typically, the mesh sizes of the solutions include 10^4 - 10^5 points, with a relative accuracy of 10^{-10} for both functions and derivatives. To implement the realistic equations of state, we used a monotonic cubic Hermite interpolation of the data points for the tabulated EOS, or alternatively, a piecewise polytropic interpolation as described in [46]. The results obtained with the two methods proved to be in very good agreement, pointing to the correctness of the calculations.

3.1 Time evolution of the axial perturbation equation

We start our discussion of the numerical results by examining the axial oscillations of neutron stars in GR and $f(R)$ gravity via time evolution of the time-dependent equation (13). We here concentrate mainly on the characteristics of the problem that can be extracted solely from the time evolution including a comparison with the results from the complex scaling method, and leave the detailed discussion of the behavior of the oscillation frequencies, damping times and universal relations for the next sections.

We evolved Eq. (13) for a given period of time imposing a Gaussian pulse as initial data¹. The frequency was calculated from the obtained waveform via Fourier transformation of the signal. The damping times were obtained by fitting the peaks of the signal with an exponential function. The coefficient in this fitting exponent is the imaginary part of the frequency, which is related to the damping time via $\tau = 1/\omega_I$.

We studied neutron star models with a realistic EOS, namely the APR4 EOS [47]. The presented waveforms were extracted at about 200 km physical distance from the star as defined according to Eq. (8). This distance was chosen in such a way that it is on one hand far enough from the star, and on the other hand the outer boundary of the numerical integration was located at much larger radial distances, so that any contamination from ingoing waves (due to the finiteness of the computational domain) was avoided.

The results we present in this subsection are for very massive neutron stars only. The reason is that the damping time of the considered modes increases with the increase of the compactness which leads to a larger number of oscillations to be observed before the signal dies out. Since the axial modes have very small damping times in general, the number of oscillations is not that large even for the most massive models. For the considered EOS, one

¹We used a Gaussian pulse for convenience. The results for the axial mode frequencies should be independent of the form of the initial pulse.

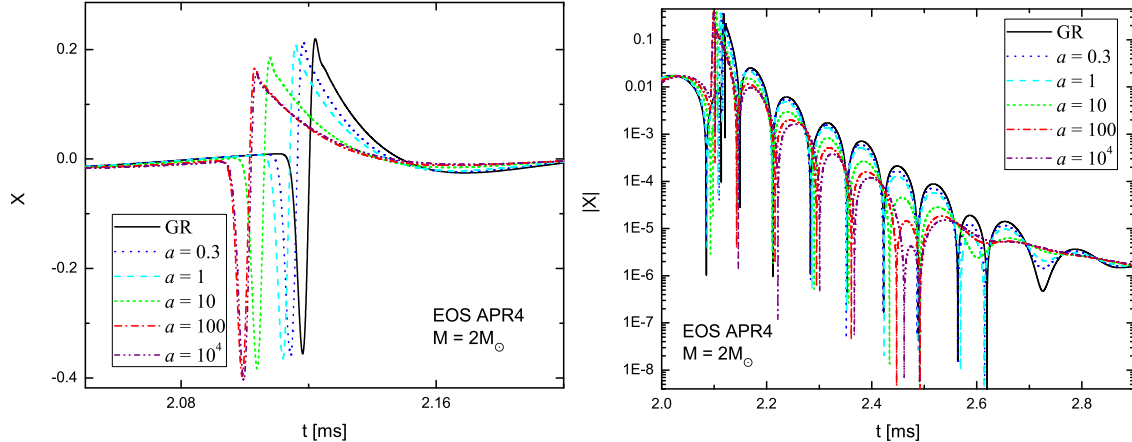


Figure 1: The observed signal at approximately 200 km physical distance from the star obtained via time evolution of the time-dependent perturbation equation. The studied neutron star models are obtained with EOS APR4, mass $M = 2M_{\odot}$ and for different values of the parameter a between GR (black) and $a = 10^4$ (purple). (*left*) The signal is presented as a function of time in milliseconds. (*right*) The absolute value of the same signal is shown on a logarithmic scale as a function of time.

can determine the oscillation frequencies and damping times with good accuracy only for masses of the order of two solar masses. Since one of the main motivations for performing time evolution calculations is to verify the results from solving the time-independent problem via the complex scaling method, we have chosen to work with masses of $2M_{\odot}$ and above in order to have high enough accuracy.

The waveforms for neutron star models with masses $M = 2.0M_{\odot}$ and $M = 2.15M_{\odot}$ and for the fundamental $l = 2$ curvature mode are presented in Figs. 1 and 2. In the left panels of both figures the signal is presented as a function of time, and in the right panels the absolute value of the signal is shown on a logarithmic scale as a function of time. As commented, the signal is extracted at a physical distance from the star which is roughly equal to 200 km.

The figures show the dependence of the arrival time of the signal on the free parameter a . As expected, the maximal deviation from GR, and hence the shortest arrival time, occurs for the largest value of a considered, and the arrival time gets closer to the GR value when a decreases. This effect arises from two sides. First, we extract the signal at a fixed physical distance, that differs from the coordinate one according to Eq. (8). Second, the effective potential of the perturbation equation (15) is influenced by the presence of a scalar field (or R^2 modification of GR). A similar effect of a delay in the arrival time of the signal is observed also in [22] for the case of scalar-tensor theories with a massless scalar field.

In Table 1 we present the oscillation frequencies and damping times extracted from the time evolution results presented in Figs. 1 and 2 together with the results obtained by solving the boundary value problem. As one can see there is a good agreement between the results for the oscillation frequencies and damping times obtained with both methods. The maximal

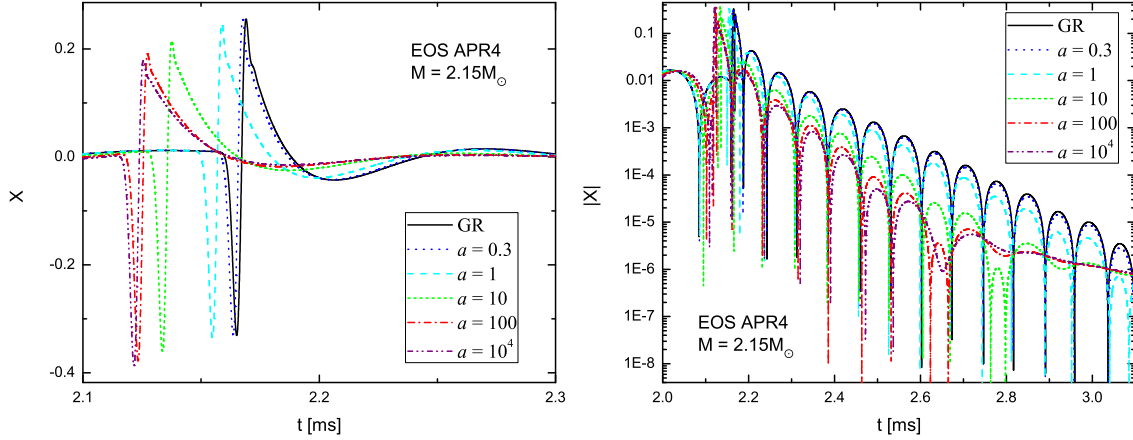


Figure 2: The observed signal at approximately 200 km physical distance from the star obtained via time evolution of the time-dependent perturbation equation. The studied neutron star models are obtained with EOS APR4, mass $M = 2.15M_{\odot}$ and for different values of the parameter a between GR (black) and $a = 10^4$ (purple). (*left*) The signal is presented as a function of time in milliseconds. (*right*) The absolute value of the same signal is shown on a logarithmic scale as a function of time.

deviation between both methods is about 3% for all of the considered models².

The data in the table show that both the frequencies of the modes and the damping times decrease with increasing a . This leads to a serious decrease of the number of oscillations observed in the signal in Figs. 1 and 2 for large a due to the fast damping. We leave further comments on the behavior of these quantities for the following subsections.

Model	Time evolution	BVP	Time evolution	BVP
	ω_R [kHz]	ω_R [kHz]	τ [μ s]	τ [μ s]
GR	7.222	7.300	61.999	62.618
$a = 0.3$	7.259	7.277	61.194	61.637
$a = 1$	7.175	7.232	59.265	59.728
$a = 10$	6.909	7.049	54.612	54.291
$a = 10^2$	6.820	6.891	51.902	50.770
$a = 10^4$	6.578	6.803	48.266	49.034

Table 1: The oscillation frequencies and the damping times of neutron stars with EOS APR4, mass $M = 2M_{\odot}$ and for different values of the parameter a between GR and $a = 10^4$. For comparison results obtained with the time evolution and the time-independent boundary value problem (BVP) are presented.

²This deviation might increase with the decrease of the stellar compactness due to the low accuracy of the results coming from the decrease of the damping time. That is why we have chosen to work with higher mass models as commented above.

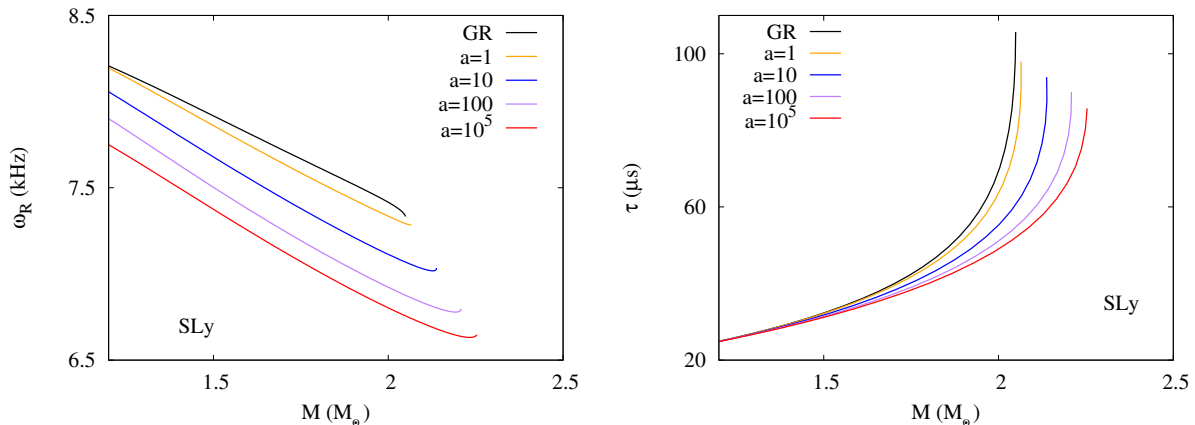


Figure 3: (*left*) Frequency ω_R (in units of kHz) of the fundamental $l = 2$ curvature mode versus the mass (in units of the solar mass M_\odot) of neutron stars with the SLy equation of state and different values of the parameter a varying between GR (black) and $a = 10^5$ (red). (*right*) A similar figure showing the damping time τ (in μs).

3.2 Boundary value problem

3.2.1 Axial quasi-normal mode spectrum for different EOS and values of a

In this subsection we present the dependence of the spectrum of QNMs on the parameter a obtained by solving the time-independent perturbation equation (15) via the complex scaling method. We consider a set of ten realistic equations of state describing different matter contents. To label the EOS we follow the nomenclature used previously in [24, 39, 40, 48]. Some of the EOS include purely nuclear matter (SLy, APR4), others hyperon matter (GNH3, H4, BHZBM, WCS1-2), or a mixture of quark and nuclear matter (ALF2-4, WSHPS3). We now focus on the fundamental $l = 2$ curvature mode.

As an example of the typical effect of the R^2 term on the QNMs, we present in Fig. 3 the fundamental $l = 2$ curvature mode for the SLy EOS. In Fig. 3 (left panel) we show the frequency ω_I in kHz versus the total mass of the neutron star in M_\odot . In black we show the frequencies for the GR case and in red for the $a = 10^5$ case, and in between for further values of the parameter a (in orange $a = 1$, in blue $a = 10$, and in purple $a = 100$). In general the frequency is maximal in GR and decreases as the value of a is increased, becoming minimal for the massless Brans-Dicke theory. Note that since the maximum mass increases with the value of a , the lowest frequencies are reached by the massless Brans-Dicke neutron stars with masses close to the maximum. Similarly, in Fig. 3 (right panel) we show the damping time τ in μs as a function of the total mass. The damping time is largest in GR, and decreases with increasing value of a . Interestingly, for low mass configurations the values of the damping time become rather independent of a . The damping time increases monotonically with the mass in all cases. These features are present independently of the equation of state. In each panel of Fig. 4 we show the frequency ω_R as a function of the total mass for a different EOS and several values of a . Similarly in Fig. 5 we show the damping time τ .

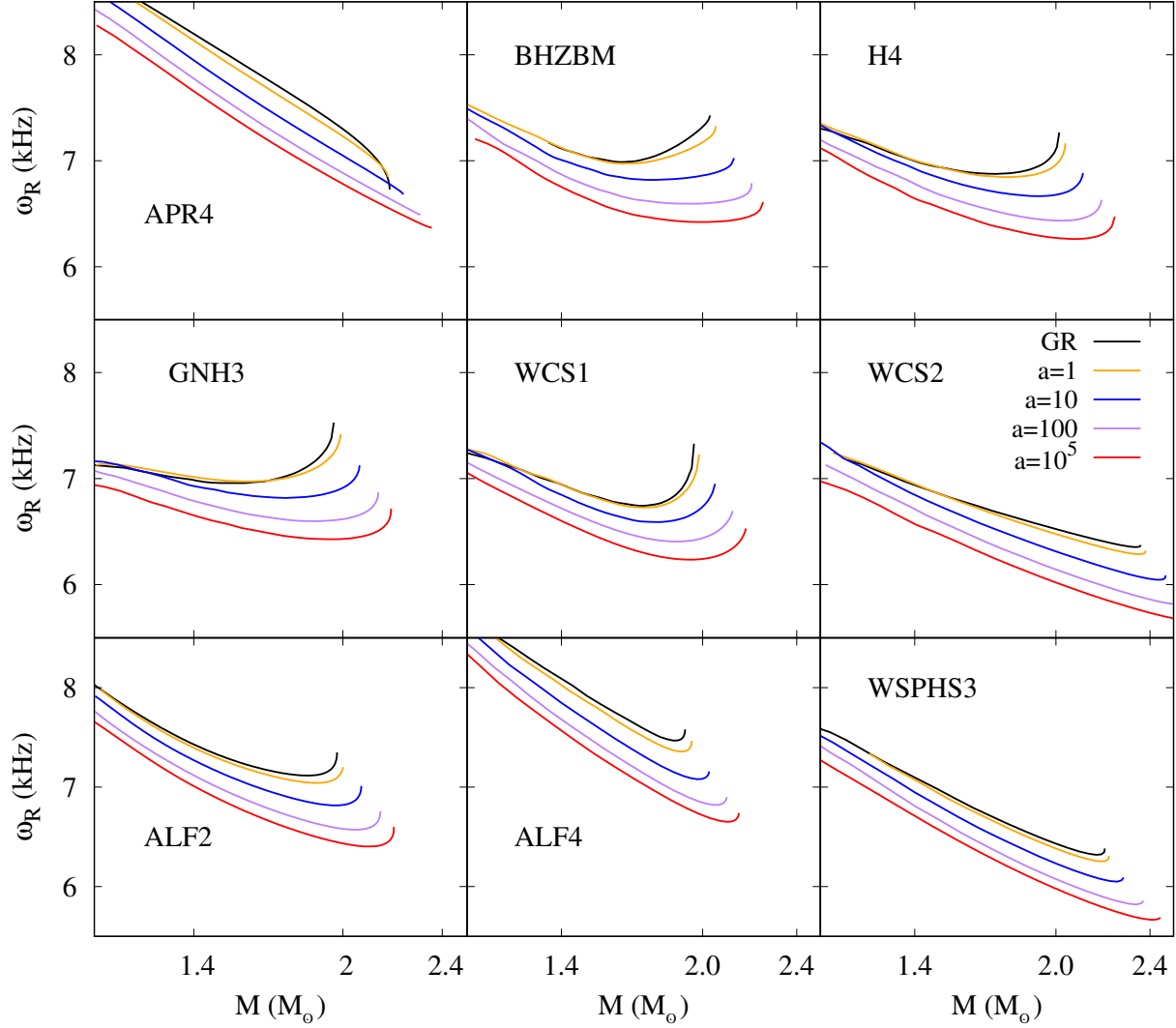


Figure 4: Frequency ω_R (in units of kHz) of the fundamental $l = 2$ curvature mode versus the mass (in units of the solar mass M_\odot) of neutron stars for different values of the parameter a between GR (black) and $a = 10^5$ (red). Each panel corresponds to a different equation of state.

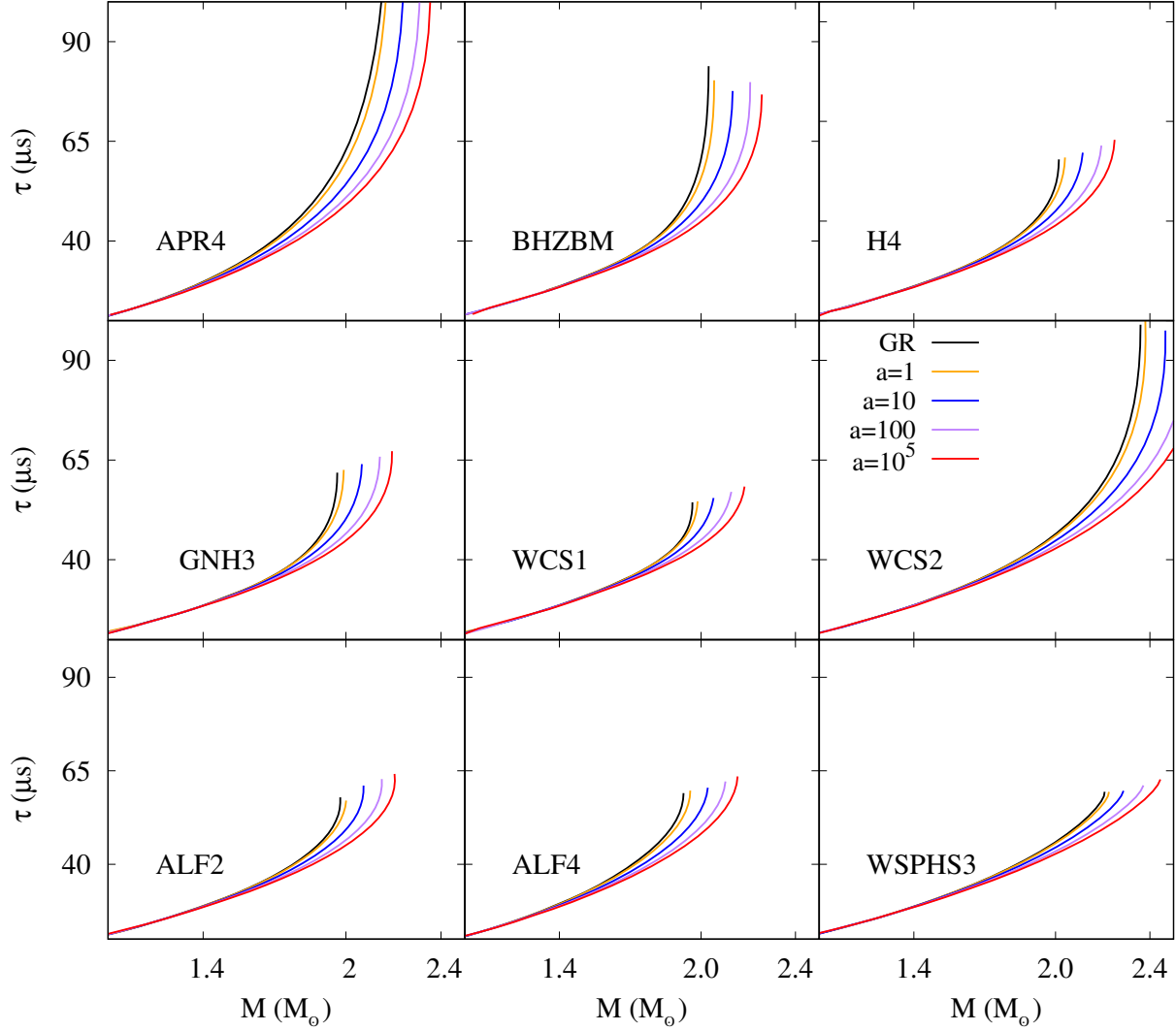


Figure 5: Damping time τ (in units of μs) of the fundamental $l = 2$ curvature mode versus the mass (in units of the solar mass M_{\odot}) of neutron stars for different values of the parameter a between GR (black) and $a = 10^5$ (red). Each panel corresponds to a different equation of state.

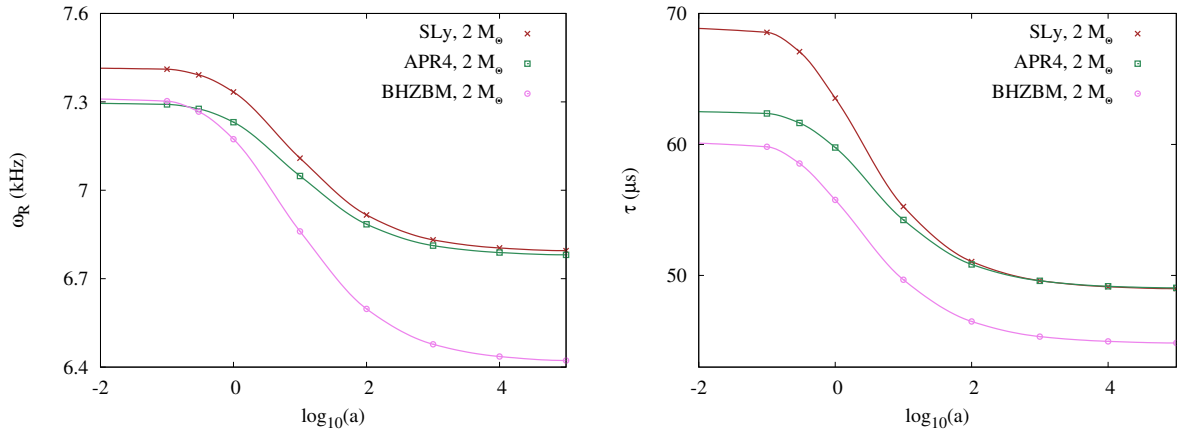


Figure 6: (*left*) Frequency ω_R (in units of kHz) of the fundamental $l = 2$ curvature mode versus the parameter a on a logarithmic scale for a neutron star mass of $2 M_\odot$ and three EOS (Sly brown, APR4 green, BHZBM purple). (*right*) A similar figure for the damping time τ (μs).

In Fig. 6 we show the frequency ω_R (left panel) and the damping time τ (right panel) as a function of the parameter a for several EOS (SLy in brown, APR4 in green and BHZBM in purple) and for a fixed value of the total mass, $M = 2M_\odot$. Both the frequency and the damping time decrease monotonically as the value of a increases. This behaviour is observed for large values of the mass (i.e., larger compactness). However, for small values of the mass (around $1M_\odot$), this behaviour can change for some equations of state, with the frequency slightly increasing for small values of a , as can be seen in Fig. 4 (e.g., for GNH3 and WCS1). The limit $a \rightarrow 0$ leads to the corresponding GR value of the mode, while the limit $a \rightarrow \infty$ gives the massless Brans-Dicke value.

3.2.2 Universal relations

Let us now address (approximate) universal relations for the rescaled frequencies and the rescaled damping times [37, 24, 38, 35, 36]. In Fig. 7 (left panel) we exhibit the frequency ω_R rescaled with the radius R_s of the star versus the compactness M/R_s of the star. The results are shown for GR, and for $f(R)$ theory with $a = 10$ and $a = 10^5$. The three sets of results are fitted with the same phenomenological relation, where different coefficients are obtained, namely

$$\omega_R[\text{kHz}] \cdot R_s[\text{km}] = \begin{cases} (105.39 \pm 0.14) - (344.2 \pm 2.8) \left(\frac{M}{R_s}\right)^2 & \text{GR} \\ (101.19 \pm 0.14) - (310.0 \pm 3.0) \left(\frac{M}{R_s}\right)^2 & a = 10 \\ (53.20 \pm 0.42) - (203.7 \pm 7.8) \left(\frac{M}{R_s}\right)^2 & a = 10^5 \end{cases} \quad (21)$$

In all cases the deviation from universality (i.e., the best fit) is less than 5%, as seen in the bottom panel of the figure. As expected, the normalized frequency is highest for GR,

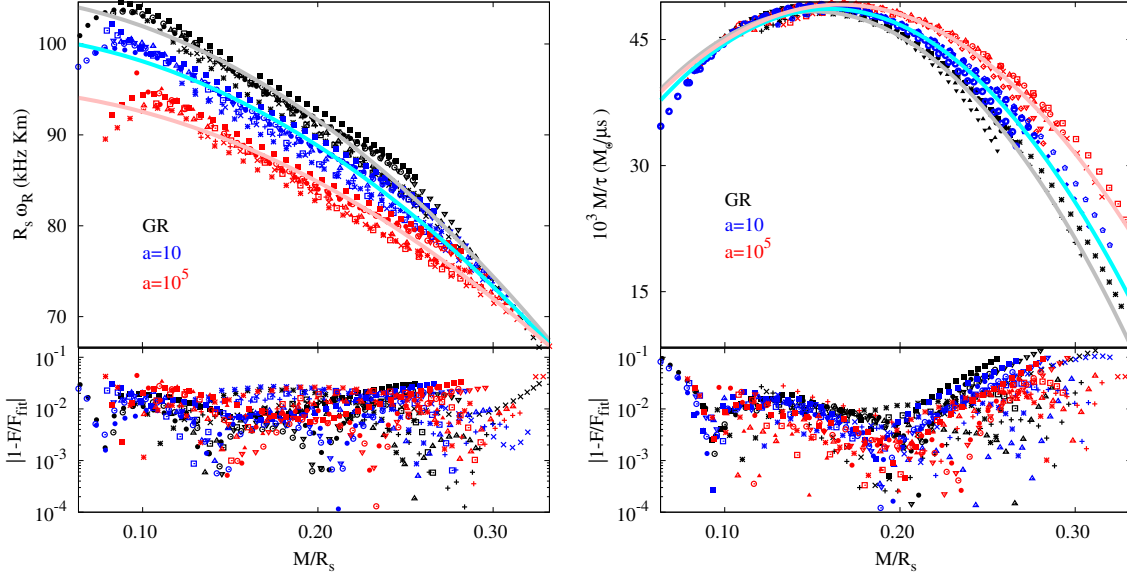


Figure 7: (*left*) Frequency ω_R scaled with the radius R_s of the star ($\text{kHz} \cdot \text{km}$) versus compactness M/R_s . (*right*) Inverse of the damping time τ scaled with respect to the mass of the star ($M_\odot/\mu\text{s}$) versus compactness M/R_s in black for GR, in blue for $a = 10$, and in red for $a = 10^5$. The solid lines correspond to the fits (21) and (22) (in grey for GR, in cyan for $a = 10$ and in pink for $a = 10^5$).

decreases with increasing a , and is smallest for $a = 10^5$.

In Fig. 7 (right panel) we exhibit the inverse of the damping time τ rescaled with the mass of the star versus the compactness of the models. Again, the phenomenological relation has the same form as in GR but with different coefficients

$$10^3 \frac{M[M_\odot]}{\tau[\mu\text{s}]} = \begin{cases} (20.80 \pm 0.56) + (365.6 \pm 6.0) \frac{M}{R_s} - (1213 \pm 15) \left(\frac{M}{R_s}\right)^2 & \text{GR} \\ (18.78 \pm 0.45) + (374.0 \pm 5.0) \frac{M}{R_s} - (1170 \pm 13) \left(\frac{M}{R_s}\right)^2 & a = 10 \\ (21.99 \pm 0.53) + (327.4 \pm 5.5) \frac{M}{R_s} - (986 \pm 13) \left(\frac{M}{R_s}\right)^2 & a = 10^5 \end{cases} \quad (22)$$

The deviations from universality are higher in this case with models for maximal compactness showing deviations of up to about 10%. The lowest normalized inverse damping times are present for GR, and they increase with the increase of the parameter a . Both phenomenological relations show significant maximal deviations from GR in different parts of the compactness scale, which may prove quite useful for deriving constraints on the parameter of the theory, once the observations will reach the necessary accuracy.

An alternative universal relation for the frequency is shown in Fig. 8 (left), where the frequency is scaled with the total mass of the star instead of the radius. The corresponding

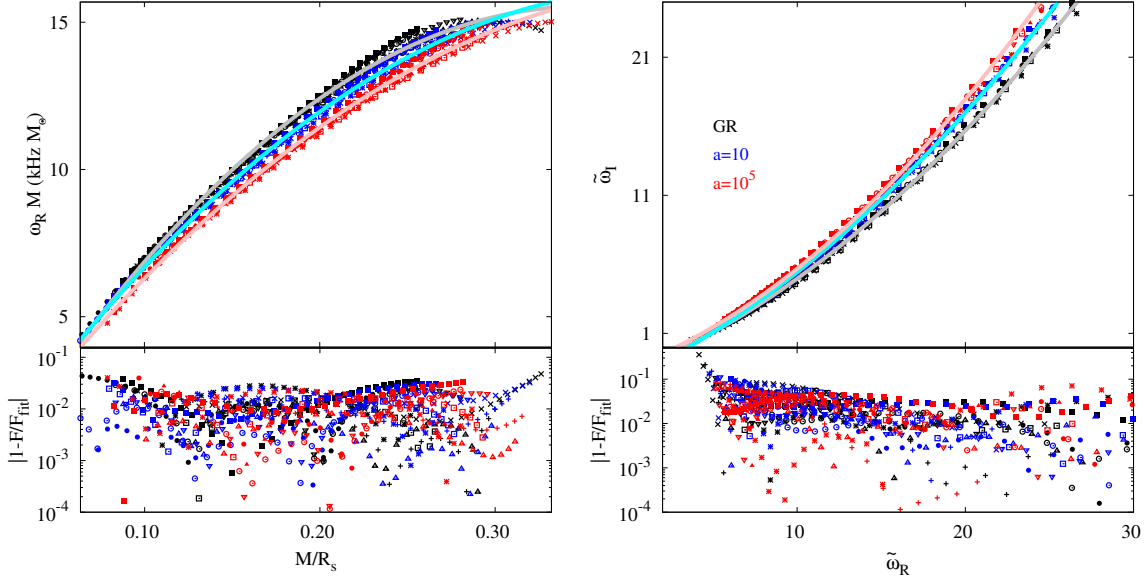


Figure 8: (left) Frequency ω_R scaled with the mass M of the star ($\text{kHz} \cdot M_\odot$) versus compactness M/R_s . (right) Imaginary part $\tilde{\omega}_I$ versus real part $\tilde{\omega}_R$ of the QNM mode, both scaled with the square root of the central pressure, for GR (red), $a = 10$ (blue) and $a = 10^5$ (red). The solid lines correspond to the fits (23) and (24) (in grey for GR, in cyan for $a = 10$ and in pink for $a = 10^5$).

phenomenological relation is

$$\omega_R[\text{kHz}] \cdot M[M_\odot] = \begin{cases} (-1.455 \pm 0.108) + (97.03 \pm 1.15) \frac{M}{R_s} - (138.5 \pm 2.9) \left(\frac{M}{R_s}\right)^2 & \text{GR} \\ (-0.725 \pm 0.085) + (84.62 \pm 0.96) \frac{M}{R_s} - (106.0 \pm 2.5) \left(\frac{M}{R_s}\right)^2 & a = 10 \\ (-0.660 \pm 0.108) + (78.73 \pm 1.11) \frac{M}{R_s} - (91.3 \pm 2.7) \left(\frac{M}{R_s}\right)^2 & a = 10^5 \end{cases} \quad (23)$$

which possesses a good EOS universality, comparable to the relation (21).

Finally, in Fig. 8 (right) we show another interesting universal relation, which holds between the real and the imaginary part of the QNMs, when both parts are scaled with respect to the central pressure of the models [39, 40, 24]. Thus defining the dimensionless scaled quantity $\tilde{\omega} = \omega/\sqrt{\bar{p}_0}$, where \bar{p}_0 is the central pressure, one finds the phenomenological relation

$$\tilde{\omega}_I = \begin{cases} (-1.821 \pm 0.067) + (0.482 \pm 0.010)\tilde{\omega}_R + (0.0197 \pm 0.0003)\tilde{\omega}_R^2 & \text{GR} \\ (-2.278 \pm 0.060) + (0.578 \pm 0.007)\tilde{\omega}_R + (0.0192 \pm 0.0002)\tilde{\omega}_R^2 & a = 10 \\ (-1.502 \pm 0.114) + (0.465 \pm 0.016)\tilde{\omega}_R + (0.0254 \pm 0.0004)\tilde{\omega}_R^2 & a = 10^5 \end{cases} \quad (24)$$

Also this relation shows a rather good EOS universality with deviations up to about 10%.

4 Conclusions

We considered axial quasi-normal modes of neutron stars in $f(R)$ gravity with various realistic equations of state describing pure nuclear matter, hyperon matter, and a mixture of quark and nuclear matter. The equation for the axial quasi-normal modes of neutron stars in $f(R)$ gravity were derived, and the QNM frequencies were calculated numerically. Most studies of the spectrum and the universal (EOS independent) relations were performed on the basis of the results obtained by solving the boundary value problem for the time-independent equation. In addition, in order to verify the results and to understand the problem in more detail, a time evolution of the time-dependent perturbation equation was performed.

With the time evolution method we studied the wave profiles and their deviations from the pure GR ones for several values of the free parameter of the theory for neutron star models with a fixed mass. From the obtained signal we extracted the oscillation frequency and the damping times. The results were compared to the ones from the boundary value problem, yielding very good agreement between both methods.

We employed the time-independent perturbation equation to obtain the frequencies and the damping times for sequences of models in GR and $f(R)$ gravity and analyzed the results in order to reveal the effect of the modification of the theory and the value of its free parameter a on the oscillation frequencies and the damping times. The effect on the frequencies found for the largest considered value of $a = 10^5$ is a decrease of the frequency of about 8 to 10% compared to GR, and it is more or less constant for all considered masses. The damping times decrease as well when increasing the parameter a . Interestingly, the damping times are very close for all values of a for small neutron star masses, and the deviation increases with the mass of the models.

We further showed that the previously found universal relations in GR remain to a large extent also EOS independent for $f(R)$ gravity. However, there are qualitative differences that increase with increasing parameter a . Expectedly, the maximal deviation arises for the maximal value of a considered, $a = 10^5$, and the relations tend to the GR ones when a is decreased. Clearly, one should next also study the polar modes of the models in $f(R)$ gravity, as well as the fluid modes. A first step in the latter direction has already been taken [49].

Acknowledgements

We would like to thank K. Kokkotas for valuable comments. JLBS and JK would like to acknowledge support by the DFG Research Training Group 1620 *Models of Gravity* and the COST Action CA16104. KS, SY, and DD would like to thank for support by the COST Action CA16214. DD would like to thank the European Social Fund, the Ministry of Science, Research and the Arts Baden-Württemberg for the support. DD is indebted to the Baden-Württemberg Stiftung for the financial support of this research project by the Eliteprogramme for Postdocs.

References

- [1] B. P. Abbott *et al.* Phys. Rev. Lett. **116**, no. 6, 061102 (2016)
- [2] B. P. Abbott *et al.* Phys. Rev. Lett. **116**, no. 24, 241103 (2016)
- [3] B. P. Abbott *et al.* Phys. Rev. Lett. **119**, no. 14, 141101 (2017)
- [4] B. P. Abbott *et al.* Phys. Rev. Lett. **118**, no. 22, 221101 (2017)
- [5] B. P. .Abbott *et al.* Astrophys. J. **851**, no. 2, L35 (2017)
- [6] B. P. Abbott *et al.* Phys. Rev. Lett. **119**, no. 16, 161101 (2017)
- [7] B. P. Abbott *et al.* Astrophys. J. **848**, no. 2, L12 (2017)
- [8] P. Demorest, T. Pennucci, S. Ransom, M. Roberts and J. Hessels, Nature **467**, 1081 (2010)
- [9] J. Antoniadis *et al.*, Science **340** (2013) 6131
- [10] J. M. Lattimer and A. W. Steiner, Astrophys. J. **784**, 123 (2014)
- [11] F. Özel and P. Freire, Ann. Rev. Astron. Astrophys. **54**, 401 (2016)
- [12] E. R. Most, L. R. Weih, L. Rezzolla and J. Schaffner-Bielich, arXiv:1803.00549 [gr-qc].
- [13] E. Berti *et al.*, Class. Quant. Grav. **32**, 243001 (2015)
- [14] E. Berti, K. Yagi and N. Yunes, arXiv:1801.03208 [gr-qc]
- [15] E. Berti, K. Yagi, H. Yang and N. Yunes, arXiv:1801.03587 [gr-qc]
- [16] K. D. Kokkotas and B. G. Schmidt, Living Rev. Rel. **2** (1999) 2
- [17] H. P. Nollert, Class. Quant. Grav. **16** (1999) R159
- [18] V. Ferrari and L. Gualtieri, Gen. Rel. Grav. **40** (2008) 945
- [19] K. D. Kokkotas and B. F. Schutz, Mon. Not. Roy. Astron. Soc. **255** (1992) 119
- [20] K. D. Kokkotas, Mon. Not. Roy. Astron. Soc. **268**, 1015 (1994)
- [21] N. Andersson, K. D. Kokkotas and B. F. Schutz, Mon. Not. Roy. Astron. Soc. **274** (1995) 1039
- [22] H. Sotani and K. D. Kokkotas, Phys. Rev. D **71** (2005) 124038
- [23] H. Sotani, Phys. Rev. D **80**, 064035 (2009)

- [24] J. L. Blázquez-Salcedo, L. M. González-Romero, J. Kunz, S. Mojica and F. Navarro-Lérida, *Phys. Rev. D* **93**, no. 2, 024052 (2016)
- [25] J. L. Blázquez-Salcedo and K. Eickhoff, arXiv:1803.01655 [gr-qc]
- [26] T. P. Sotiriou and V. Faraoni, *Rev. Mod. Phys.* **82**, 451 (2010)
- [27] A. De Felice and S. Tsujikawa, *Living Rev. Rel.* **13**, 3 (2010)
- [28] S. Capozziello and M. De Laurentis, *Phys. Rept.* **509**, 167 (2011)
- [29] S. S. Yazadjiev, D. D. Doneva, K. D. Kokkotas and K. V. Staykov, *JCAP* **1406** (2014) 003
- [30] K. V. Staykov, D. D. Doneva, S. S. Yazadjiev and K. D. Kokkotas, *JCAP* **1410** (2014) no.10, 006
- [31] S. S. Yazadjiev, D. D. Doneva and K. D. Kokkotas, *Phys. Rev. D* **91** (2015) no.8, 084018
- [32] A. V. Astashenok, S. D. Odintsov and A. de la Cruz-Dombriz, *Class. Quant. Grav.* **34**, no. 20, 205008 (2017)
- [33] K. Yagi and N. Yunes, *Phys. Rept.* **681**, 1 (2017)
- [34] D. Doneva and G. Pappas, arXiv:1709.08046 [gr-qc]
- [35] N. Andersson and K. D. Kokkotas, *Phys. Rev. Lett.* **77** (1996) 4134
- [36] N. Andersson and K. D. Kokkotas, *Mon. Not. Roy. Astron. Soc.* **299** (1998) 1059
- [37] K. D. Kokkotas, T. A. Apostolatos and N. Andersson, *Mon. Not. Roy. Astron. Soc.* **320** (2001) 307
- [38] O. Benhar, V. Ferrari and L. Gualtieri, *Phys. Rev. D* **70** (2004) 124015
- [39] J. L. Blázquez-Salcedo, L. M. González-Romero and F. Navarro-Lérida, *Phys. Rev. D* **87**, no. 10, 104042 (2013)
- [40] J. L. Blázquez-Salcedo, L. M. González-Romero and F. Navarro-Lérida, *Phys. Rev. D* **89**, no. 4, 044006 (2014)
- [41] J. Naf and P. Jetzer, *Phys. Rev. D* **81** (2010) 104003
- [42] G. Álvarez and R. J. Damburg and H.J. Silverstone, *Phys. Rev. A* **44**, no. 5, 3060 (1991)
- [43] S. Chandrasekhar and S. L. Detweiler, *Proc. Roy. Soc. Lond. A* **344**, 441 (1975)
- [44] N. Andersson, *Astrophys. J.* **502**, 708 (1998)
- [45] U. Ascher, J. Christiansen and R. D. Russell, *Math. Comput.* **33**, no. 146, 659 (1979)

- [46] J. S. Read, B. D. Lackey, B. J. Owen and J. L. Friedman, Phys. Rev. D **79**, 124032 (2009)
- [47] A. Akmal, V. R. Pandharipande and D. G. Ravenhall, Phys. Rev. C **58**, 1804 (1998)
- [48] Z. Altaha Motahar, J. L. Blázquez-Salcedo, B. Kleihaus and J. Kunz, Phys. Rev. D **96**, no. 6, 064046 (2017)
- [49] K. V. Staykov, D. D. Doneva, S. S. Yazadjiev and K. D. Kokkotas, Phys. Rev. D **92** (2015) no.4, 043009